Journal of Chemical Neuroanatomy 98 (2019) 131–138

Contents lists available at ScienceDirect

Journal of Chemical Neuroanatomy

journal homepage: www.elsevier.com/locate/jchemneu

Heterogeneous expression patterns of fibronectin in the mouse subiculum

Tetsuhiko Kashima[a], Asako Noguchi[a], Yuji Ikegaya[a,b], Nobuyoshi Matsumoto[a,*]

[a] Graduate School of Pharmaceutical Sciences, The University of Tokyo, Tokyo, 113-0033, Japan
[b] Center for Information and Neural Networks, National Institute of Information and Communications Technology, Suita City, Osaka, 565-0871, Japan

ARTICLE INFO

Keywords:
Subiculum
Fibronectin
Dorsoventral axis
Immunohistochemistry
Heterogeneity
Mouse

ABSTRACT

The subiculum displays as much anatomical and physiological heterogeneity as the hippocampus. Recent studies suggest that the subiculum is also diverse in terms of gene expression. However, few studies have investigated the heterogeneity of the entire subiculum. To address this issue, we focused on fibronectin because its mRNA (FN1 mRNA) is expressed in the dorsal and ventral subiculum. We immunohistochemically characterized the intracellular expression of fibronectin in the entire subiculum along three axes (*i.e.*, the dorsoventral, proximodistal, and superficial-deep axes). We first confirmed that FN1 mRNA is translated into protein inside cells. Moreover, we found that fibronectin was expressed evenly in the pyramidal cell layer of the dorsal subiculum, whereas in the ventral subicular pyramidal field, fibronectin was most concentrated in the superficial, distal corner. These results suggest that excitatory neurons labeled by fibronectin are more localized in the ventral subiculum than in the dorsal subiculum. Therefore, fibronectin may be useful as an indicator for studying the heterogeneity of principal cells in the subiculum.

1. Introduction

The hippocampal formation, which is composed of the hippocampus (*i.e.*, the hippocampus proper and dentate gyrus) and the subiculum (van Strien et al., 2009), plays a crucial role in episodic and spatial memory. The subiculum has been the focus of fewer anatomical, physiological and behavioral studies than the hippocampus. Recent studies have suggested that the subiculum has a unique role in information processing (Matsumoto et al., 2018; Norimoto et al., 2013). In addition, the subiculum and hippocampus have distinct cytoarchitectures and laminar structures. Furthermore, the principal cells in the distal and proximal portions of the subiculum differ in their afferent and efferent innervation (Honda and Ishizuka, 2015; Honda and Shibata, 2017) and their firing properties (Jarsky et al., 2008). Although these studies characterized the subiculum to some extent, few studies have focused on the entire (*i.e.*, dorsal and ventral) subiculum.

Transcriptome studies demonstrate that the subiculum exhibits neuroanatomical heterogeneity (Cembrowski et al., 2018a); however, the heterogeneity of the expression patterns of proteins has been poorly investigated in the subiculum. Therefore, to characterize the heterogeneity of the entire subiculum (Bienkowski et al., 2018), we took advantage of an immunohistochemical method. Among proteins that may be expressed specifically in the subiculum (Ishihara and Fukuda, 2016), the current study focused on fibronectin because its mRNA is widely expressed in principal neurons in the subiculum (Cembrowski et al., 2018b) and because fibronectin is reported to be associated with memory (Roy et al., 2017). Nevertheless, to date, it remains unknown whether the FN1 mRNA is translated and how fibronectin protein is distributed in the subiculum. In this study, we analyzed immunohistochemical signals for fibronectin protein in the subiculum along the dorsoventral axis as well as the proximodistal and superficial-deep axes and examined the heterogeneity of the subiculum based on the expression of fibronectin.

2. Materials and methods

2.1. Animal ethics

Animal experiments were performed with the approval of the animal experiment ethics committee at the University of Tokyo (approval number: P24–10) and in accordance with the University of Tokyo guidelines for the care and use of laboratory animals. The experimental protocols were performed in accordance with the Fundamental Guidelines for the Proper Conduct of Animal Experiments and Related Activities in Academic Research Institutions (Ministry of Education, Culture, Sports, Science and Technology, Notice No. 71 of 2006), the

* Corresponding author at: Laboratory of Chemical Pharmacology, Graduate School of Pharmaceutical Sciences, The University of Tokyo, 7-3-1 Hongo, Bunkyo-ku, Tokyo, 113-0033, Japan.
E-mail address: nmatsumoto@mol.f.u-tokyo.ac.jp (N. Matsumoto).

https://doi.org/10.1016/j.jchemneu.2019.04.010
Received 21 November 2018; Received in revised form 26 April 2019; Accepted 30 April 2019
Available online 01 May 2019
0891-0618/

Standards for Breeding and Housing of and Pain Alleviation for Experimental Animals (Ministry of the Environment, Notice No. 88 of 2006) and the Guidelines on the Method of Animal Disposal (Prime Minister's Office, Notice No. 40 of 1995).

2.2. Histology

Fifteen young adult (6-week-old) male C57BL/6 J mice were anesthetized *via* intraperitoneal administration of 150 mg/ml urethane dissolved in saline. Anesthesia was confirmed *via* the lack of reflex responses to tail and toe pinch. The mice were transcardially perfused with ice-cold phosphate-buffered saline (PBS) followed by 4% paraformaldehyde in PBS, and the brains were removed. The brains were postfixed in 4% paraformaldehyde overnight, washed with PBS three times for 10 min each and horizontally ($n = 12$ mice) sectioned using a vibratome at a thickness of 100 μm from the dorsal region to the ventral region unless otherwise noted. For Fig. 5, brains were coronally ($n = 3$ mice) sectioned at a thickness of 100 μm from the anterior end to the posterior end. Among horizontally sectioned slices, the most dorsal slice for each brain was identified as the one in which the cross-sectional area of the subicular pyramidal cell layer exceeded 0.4 mm^2. The dorsoventral locations of horizontally sectioned slices were expressed relative to the most dorsal section (0 μm). We collected horizontally sectioned slices every 500 μm from 0 μm to 3000 μm (*i.e.*, seven slices per brain) and coronally sectioned slices every 300 μm from the anterior side to the posterior side. These sections covered nearly the entire subiculum area.

The sections were blocked with 5% BSA and 0.3% Triton X-100 in PBS for 60 min at room temperature. These sections were incubated with mouse primary antibody against neuronal nuclei (NeuN; 1:1000, MAB377, Merck Millipore, Billerica, MA, USA), rabbit primary antibody against fibronectin (1:400, ab2413, Abcam, Cambridge, UK (Chen et al., 2017; Reticker-Flynn et al., 2012; Worth et al., 2010; Yi et al., 2016)), and guinea pig primary antibody against vesicular glutamate transporter 2 (VGluT2) (1:1000, VGluT2-GP-Af810, Frontier Institute, Hokkaido, Japan (Ishihara and Fukuda, 2016)) in 1% BSA and 0.3% Triton X-100 in PBS for 16 h at 4 °C. The sections were washed three times for 10 min each with PBS and incubated with Alexa Fluor 488-conjugated goat secondary antibody against mouse IgG (1:500, A11001, Invitrogen, MA, USA), Alexa Fluor 594-conjugated goat secondary antibody against rabbit IgG (1:500, A11037, Invitrogen, MA, USA), and NeuroTrace 435/455 blue fluorescent Nissl stain (1:500, N21479, Thermo Fisher Scientific, MA, USA) in 1% BSA and 0.3% Triton X-100 in PBS for 1.5 h at room temperature.

To validate the specificity of the rabbit anti-fibronectin primary antibody (Fritschy, 2008; Rhodes and Trimmer, 2006), we preincubated it with native mouse fibronectin protein (ab92784, Abcam, Cambridge, UK) for 16 h at 4 °C at a concentration that was 5 times that of the antibody by weight. The preprocessed primary antibody was used to validate its antigen specificity (Fig. 2C, D).

2.3. Confocal imaging

The images (1024 × 1024 pixels, 16-bit intensity) for each region of interest were acquired at Z-intervals of 2.0 μm (10×, 40×) or 0.2 μm (100×) using an FV1200 confocal microscope (Olympus, Tokyo, Japan) equipped with 10×, 40× and 100× objectives and Z-stacked using ImageJ software (National Institutes of Health, MD, USA).

2.4. Statistics and analysis

The data were analyzed using MATLAB (MathWorks, Natick, MA, USA). The summarized data are reported as the mean ± the standard error of the mean (SEM). $P < 0.05$ was considered statistically significant. When multiple pairwise comparisons were required, we corrected the original P values with Bonferroni's correction and compared the corrected P values with 0.05.

To identify the subicular pyramidal field, we defined the CA1-subiculum boundary and the subiculum-presubiculum boundary based on the intensities of NeuN immunofluorescence. For the CA1-subiculum border, we aligned 0.4-μm^2 squares on the CA1 pyramidal cell layer along the proximal-to-distal axis and calculated the mean intensity of NeuN immunofluorescence in each square. We then defined the first square whose intensity was less than 5% of the maximum intensity as the most proximal and superficial point of the subiculum (*i.e.*, the end of the CA1 pyramidal cell layer). We drew a vertical line from this point to the CA1 pyramidal cell layer. For each section, we regarded this line as the boundary between the CA1 area and the subiculum. In addition, we defined a cytoarchitectural gap in the cell population as the subiculum-presubiculum boundary.

A given cell was regarded as a fibronectin-positive cell if fibronectin was expressed in more than 10% of the cell, as determined by fluorescence. After defining fibronectin-positive and fibronectin-negative cells, we determined the fibronectin-positive area by outlining the outermost fibronectin-positive cells. We then normalized the subicular pyramidal field and fibronectin-positive area in each slice in the following way: i) the superficial and deep borders between the subicular pyramidal cell layer and other subicular layers (*i.e.*, the molecular and polymorphic layers) were divided into one hundred quadrilaterals; ii) single quadrilaterals were transformed into congruent rectangles using a homography transformation matrix; iii) the fibronectin-positive area was similarly homography transformed; iv) we joined all the transformed rectangles so that the subicular pyramidal field became a single rectangle; v) we then joined the transformed fibronectin-positive area side-by-side in parallel. Subsequently, we calculated the density of the fibronectin-positive cells in the subicular pyramidal field in each slice and represented the densities as a pseudocolor map smoothed by a Gaussian filter ($\sigma = 0.5$, 10 times).

3. Results

We made 100-μm-thick brain sections, performed immunostaining, and manually outlined the NeuN-positive area to estimate the extent of the subicular pyramidal field along the dorsoventral axis (see Materials and methods; Fig. 1A). The subicular pyramidal fields of the most dorsal sections (0 μm) were significantly larger than those of the third sections (1000 μm) and sixth sections (2500 μm) ($P = 8.77 \times 10^{-11}$, $F_{(6,35)} = 22.9$; P (0 μm *vs.* 1000 μm) $= 3.10 \times 10^{-2}$, P (0 μm *vs.* 2500 μm) $= 1.22 \times 10^{-2}$, $n = 6$ mice; paired t-test with Bonferroni's *post hoc* correction after one-way analysis of variance (ANOVA); Fig. 1B), those of the most ventral sections (3000 μm) were significantly larger than those of the fourth sections (1500 μm) and fifth sections (2000 μm) ($P = 8.77 \times 10^{-11}$, $F_{(6,35)} = 22.9$; P (1500 μm *vs.* 3000 μm) $= 1.74 \times 10^{-2}$, P (2000 μm *vs.* 3000 μm) $= 6.85 \times 10^{-3}$, $n = 6$ mice; paired t-test with Bonferroni's *post hoc* correction after one-way ANOVA; Fig. 1B), and other pairs exhibited no significant differences (P (0 μm *vs.* 500 μm) $= 0.11$, P (0 μm *vs.* 1500 μm) $= 0.06$, P (0 μm *vs.* 2000 μm) $= 0.06$, P (0 μm *vs.* 3000 μm) $= 0.22$, P (500 μm *vs.* 1000 μm) $= 0.24$, P (500 μm *vs.* 1500 μm) > 0.5, P (500 μm *vs.* 2000 μm) > 0.5, P (500 μm *vs.* 2500 μm) > 0.5, P (500 μm *vs.* 3000 μm) > 0.5, P (1000 μm *vs.* 1500 μm) > 0.5, P (1000 μm *vs.* 2000 μm) > 0.5, P (1000 μm *vs.* 2500 μm) > 0.5, P (1000 μm *vs.* 3000 μm) > 0.5, P (1500 μm *vs.* 2000 μm) $= 0.49$, P (1500 μm *vs.* 2500 μm) > 0.5, P (2000 μm *vs.* 2500 μm) > 0.5, P (2500 μm *vs.* 3000 μm) > 0.5, $n = 6$ mice; paired t-test with Bonferroni's *post hoc* correction after one-way ANOVA).

We observed obvious fibronectin-positive fluorescent signal in both the dorsal and ventral subiculum in horizontally sectioned slices ($n = 6$ mice; Fig. 2A, B). We also found scattered fibronectin immunosignal in other subregions (Fig. 2A, B). To address whether fibronectin was expressed intracellularly or extracellularly, we took higher-magnification (100×) images of these slices. Surprisingly, the high-magnification

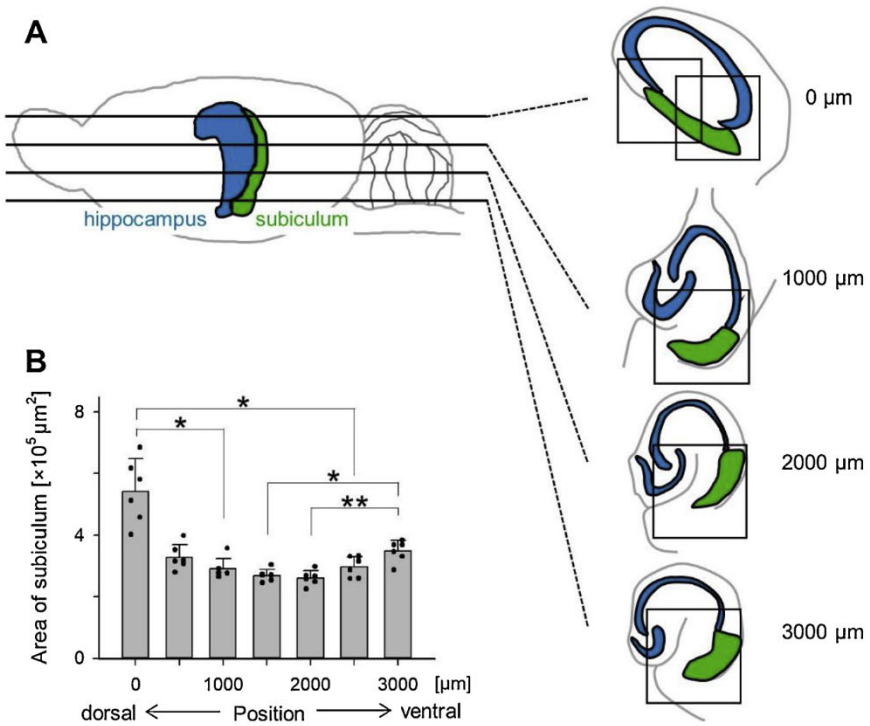

Fig. 1. Focal areas of brain sections for immunostaining. *A*, Seven 100-μm-thick sections were prepared at intervals of 500 μm from each brain. The measures indicate the distances from the most dorsal section. Sections were immunolabeled for NeuN and fibronectin and counterstained with blue fluorescent Nissl stain. Regions including the subiculum, indicated by boxes, were confocally imaged and Z-stacked. *B*, The positions of the sections are indicated by the distance from the dorsal tip (0 μm). For each dorsoventral level, we calculated the area of the subicular pyramidal field. The data are represented as the mean and SEM ($^{*}P <$ 0.05, $^{**}P <$ 0.01, paired *t*-test with Bonferroni's *post hoc* correction after one-way ANOVA, $n = 6$ mice each).

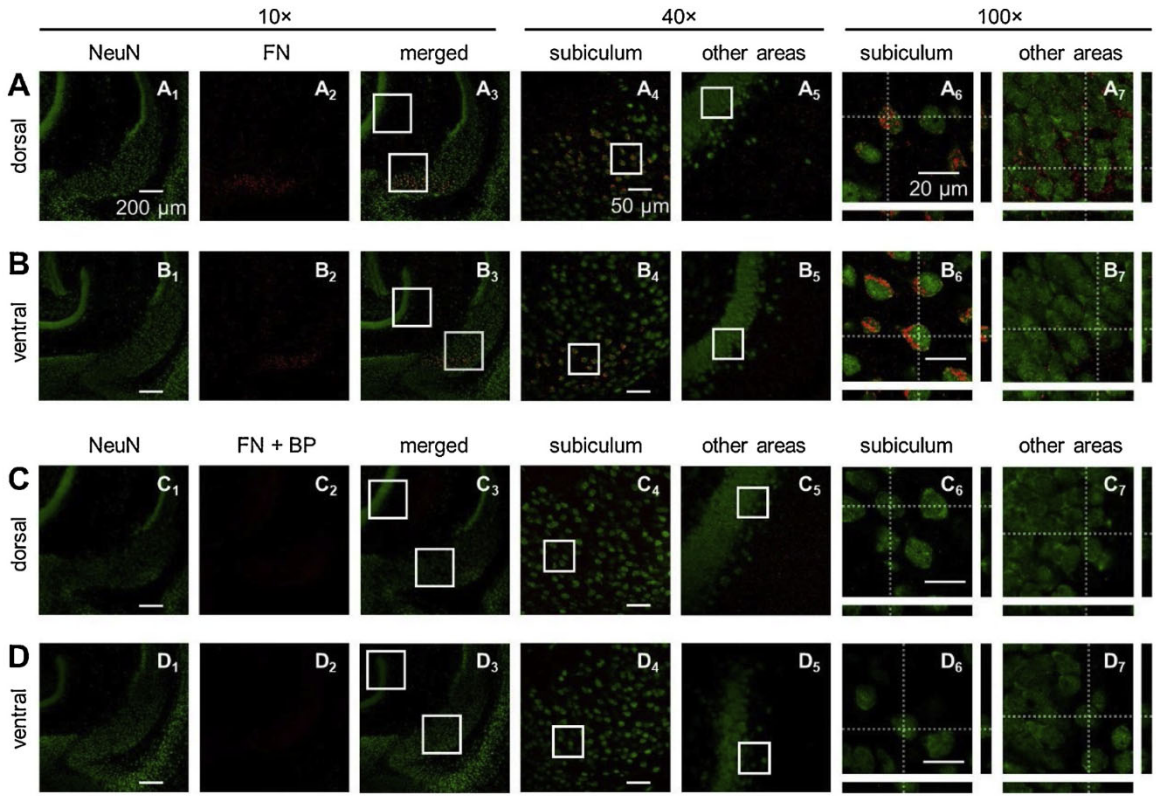

Fig. 2. Immunohistochemical signals of fibronectin in the subiculum and neighboring areas. *A*, Representative immunohistochemical images of the dorsal subiculum and its surrounding areas in a horizontal plane. Low-magnification (10×) confocal images of anti-NeuN (A_1, *green*), anti-fibronectin (A_2, *red*), and merged signal (A_3). The boxed areas (*white*) in the image in A_3 are magnified (40×) in A_4 and A_5, which correspond to the subiculum and its neighboring area, respectively. The boxed areas (*white*) in the images in A_4 and A_5 are further magnified (100×) in A_6 and A_7, respectively. A single Z-stack image of the subiculum in an X–Y plane is shown in A_6 and A_7. The images in Y–Z (*right*) and Z–X (*bottom*) planes are Z-projections in the X and Y directions, respectively. The horizontal and vertical dashed lines are orthogonal to the Y–Z (*right*) and Z–X (*bottom*) planes, respectively. Note that all fibronectin-positive cells in the subiculum expressed NeuN. *B*, The same as in *A*, but for a ventral section. *C*, The same as in *A*, but for a dorsal section immunostained by the anti-fibronectin primary antibody preincubated with a blocking peptide. No fibronectin signal was detected. *D*, The same as in *C*, but for a ventral section. *Abbreviation*: FN, fibronectin; BP, blocking peptide.

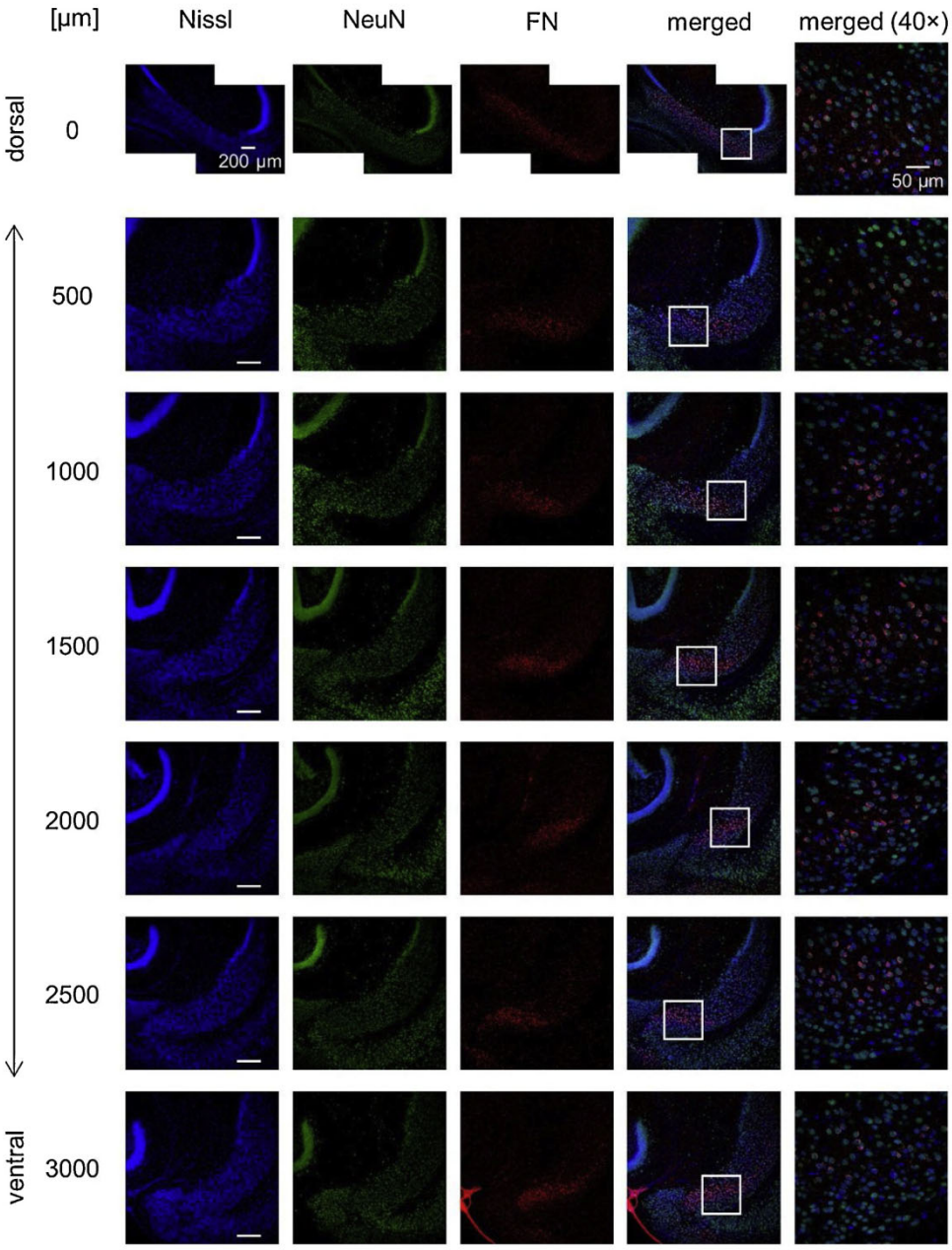

Fig. 3. Representative photographs of NeuN and fibronectin immunoreactivity in the subiculum from an adult mouse along the dorsoventral axis. In each row, confocal images of Nissl (*blue*, *left-most* column), anti-NeuN (*green*, *second*), anti-fibronectin (*red*, *third*), and merged (*fourth*) signal are superimposed. The boxed areas (*white*) in the *fourth*-column images are magnified (40×) in the *fifth* column. Different rows display photographs obtained from different dorsoventral levels, which are indicated as the distance (μm) from the most dorsal section. Experiments were repeated for all 6 animals of the same age, and the same results were obtained. *Abbreviation*: FN, fibronectin.

images confirmed that fibronectin was likely expressed within their cell bodies of subicular neurons, whereas it was expressed outside cell bodies in other brain regions (Fig. 2A, B). When the anti-fibronectin primary antibody was preincubated with a blocking peptide ($n = 3$ mice; see Materials and methods), we did not observe evident fibronectin-positive fluorescent immunosignal in any regions of dorsal or ventral sections (Fig. 2C, D). These results confirmed that both dorsal and ventral subicular neurons intracellularly expressed fibronectin, although fibronectin is generally believed to be one of the cell adhesion molecules in peripheral organs (Dixon and Burns, 1982). We then immunostained a series of horizontal sections and found expression of fibronectin within the cell bodies in all slices tested (Fig. 3).

Since fibronectin-positive cells were obviously distinguishable from fibronectin-negative cells (Fig. 4A), we defined the fibronectin-positive area as the smallest polygon that enclosed all fibronectin-positive cells in the subiculum (Fig. 4B). To normalize the fibronectin-positive areas in the subiculum, we performed a homography transformation on each manually outlined subicular pyramidal field so that it would be a rectangle and subsequently transformed the original fibronectin-positive areas using the same transformation matrix (see Materials and methods; Fig. 4C). We then estimated the density of fibronectin-positive cells within the subiculum (Fig. 4D). In this analysis, we excluded the most dorsal section (0 μm) because the subiculum in this section was merged with the CA1 area (Fig. 1A) and did not allow us to precisely define the proximodistal axis. Unexpectedly, the fibronectin-positive cells were widely distributed in the most dorsal region of the subiculum, whereas in the most ventral regions of the subiculum, they were concentrated in the distal and superficial portion (Fig. 4D). We calculated the ratio of the fibronectin-positive area to the subicular pyramidal field along the dorsoventral axis (Fig. 4E). The ratio of the fibronectin-positive area of the most dorsal sections (0 μm) was significantly larger than those of the fourth (1500 μm), fifth (2000 μm), sixth (2500 μm) and seventh (3000 μm) sections ($P = 1.21 \times 10^{-10}$, $F_{(6,35)} = 22.4$; P (0 μm *vs.* 1500 μm) $= 3.44 \times 10^{-3}$, P (0 μm *vs.* 2000 μm) $= 7.27 \times 10^{-3}$, P (0 μm *vs.* 2500 μm) $= 2.84 \times 10^{-3}$, P (0 μm *vs.* 3000 μm) $= 1.96 \times 10^{-2}$, $n = 6$ mice; paired t-test with Bonferroni's *post hoc* correction after one-way ANOVA; Fig. 4E). In addition, the ratio of the fibronectin-positive area of the second sections (500 μm)

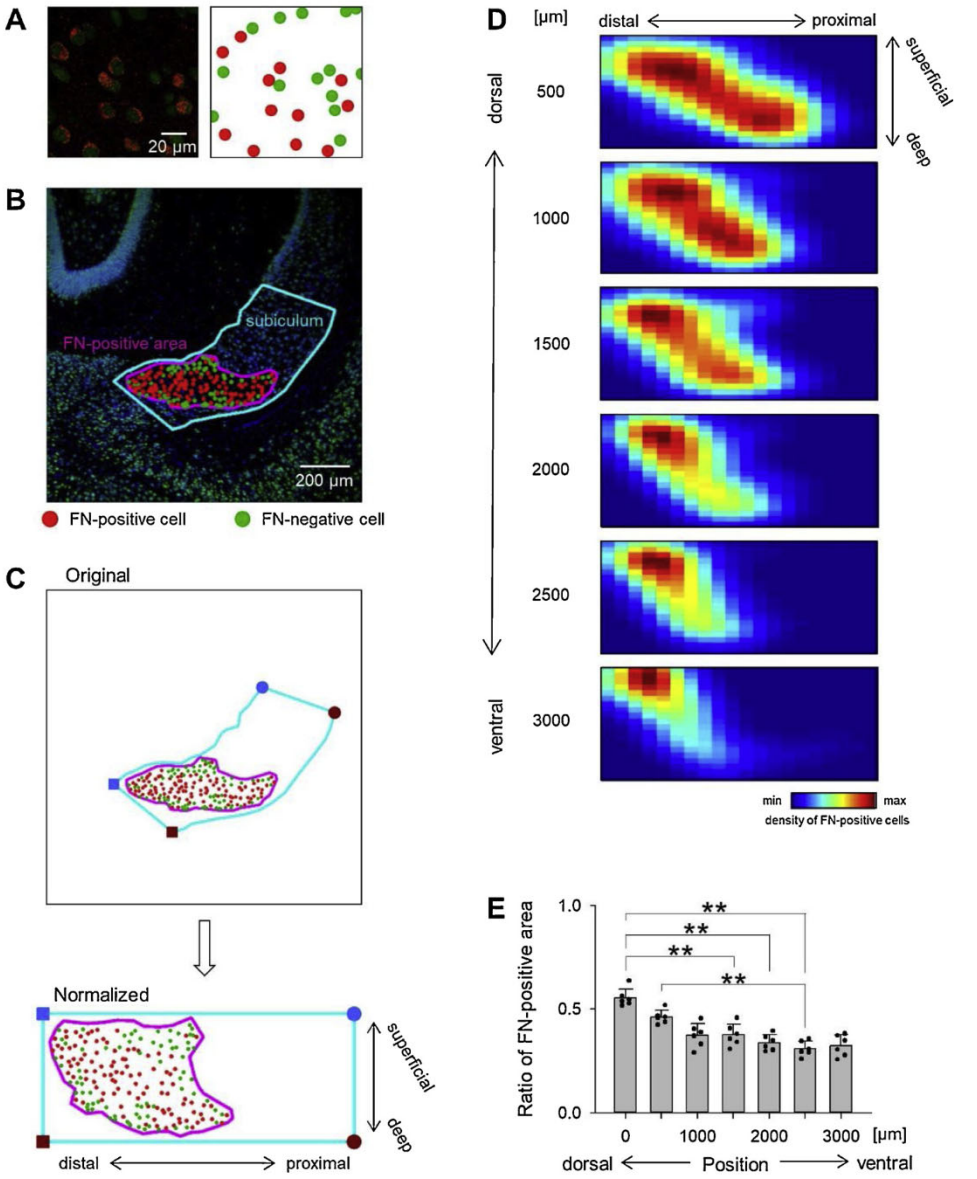

Fig. 4. Gradual transition of the fibronectin-positive area in the subiculum along the dorsoventral axis. *A*, *Left*: a representative high-magnification (40×) confocal image of the fibronectin-positive area in which anti-NeuN (*green*) and anti-fibronectin (*red*) images were superimposed. *Right*: a scatter plot in which fibronectin-positive and fibronectin-negative cells are shown in *red* and *green*, respectively. *B*, A representative low-magnification (10×) confocal image of the subiculum and its surrounding regions with Nissl (*blue*), anti-NeuN (*green*) and anti-fibronectin (*red*) and superimposed immunostaining signal. The *cyan* and *magenta* lines enclose the subicular pyramidal field and the fibronectin-positive area, respectively. The *red* and *green* circles indicate fibronectin-positive and fibronectin-negative cells, respectively, in the fibronectin-positive area as shown in *A*. *C*, *Top*: the original subicular pyramidal field, fibronectin-positive area, and fibronectin-positive and fibronectin-negative cells are extracted from *B*. The *circles* and *squares* indicate proximal and distal borders, respectively, with *blue* and *dark red* indicating superficial and deep borders, respectively, between the subicular pyramidal cell layer and other layers. *Bottom*: the normalized map to which the original map (*top*) was reshaped by the homography transformation. The *abscissa* and *ordinate* indicate the proximodistal and superficial-deep axes, respectively. *D*, Representative pseudocolor maps in which hot and cold colors indicate high and low density of fibronectin-positive cells, respectively, in the rectangular subicular domain shown in *C*. The *upper* and *lower* maps indicate the dorsal and ventral subiculum, respectively. The numbers indicate the distance (μm) from the most dorsal section (0 μm). *E*, The positions of the sections are indicated by the distance from the dorsal tip (0 μm). The ratio of the fibronectin-positive area to the entire area of the subicular pyramidal cell layer gradually decreases along the dorsal-to-ventral axis. Data are represented as the mean and SEM ($^{**}P <$ 0.01, paired *t*-test with Bonferroni's *post hoc* correction after one-way ANOVA, $n = 6$ mice each). *Abbreviation*: FN, fibronectin.

was significantly larger than those of the fifth (2000 μm), sixth (2500 μm) and seventh (3000 μm) sections ($P = 1.21 \times 10^{-10}$, $F_{(6,35)} = 22.4$; P (500 μm *vs.* 2000 μm) $= 3.03 \times 10^{-2}$, P (500 μm *vs.* 2500 μm) $= 9.29 \times 10^{-3}$, P (500 μm *vs.* 3000 μm) $= 2.66 \times 10^{-2}$, $n = 6$ mice; paired *t*-test with Bonferroni's *post hoc* correction after one-way ANOVA; Fig. 4E). In contrast, other pairs exhibited no significant differences (P (0 μm *vs.* 500 μm) $= 0.24$, P (0 μm *vs.* 1000 μm) $= 0.06$, P (500 μm *vs.* 1000 μm) $= 0.36$, P (500 μm *vs.* 1500 μm) $= 0.27$, P (1000 μm *vs.* 1500 μm) > 0.5, P (1000 μm *vs.* 2000 μm) > 0.5, P (1000 μm *vs.* 2500 μm) > 0.5, P (1000 μm *vs.* 3000 μm) > 0.5, P (1500 μm *vs.* 2000 μm) > 0.5, P (1500 μm *vs.* 2500 μm) > 0.5, P (1500 μm *vs.* 3000 μm) > 0.5, P (2000 μm *vs.* 2500 μm) > 0.5, P (2000 μm *vs.* 3000 μm) > 0.5, P (2500 μm *vs.* 3000 μm) > 0.5, $n = 6$ mice; paired *t*-test with Bonferroni's *post hoc* correction after one-way ANOVA; Fig. 4E). These results confirmed that the fibronectin-positive area of the ventral sections was smaller and more convergent than that of the dorsal sections.

When the brain was serially sectioned in a fixed plane, the geometry of the subiculum changed from one section to the next because the subiculum has a C-shaped curve in the brain. In horizontal sections, therefore, the most dorsal plane was nearly parallel to the longitudinal axis of the subiculum, whereas the most ventral plane was nearly perpendicular to the longitudinal axis of the subiculum. Thus, it was possible that the dorsoventral difference in the densities of fibronectin-positive cells depended on the planes of sectioning. To disambiguate the true dorsal-ventral differences from the sectioning differences, we immunostained coronal sections and observed the distribution pattern of fibronectin (Fig. 5). In coronal sections, we also found almost the same expression pattern of fibronectin as shown in horizontal sections (Figs. 3–5); more neurons in the dorsal subiculum expressed fibronectin than in the ventral subiculum.

To quantify the fibronectin-positive area more specifically, we counted the fibronectin-positive and fibronectin-negative cells and computed the ratio of fibronectin-positive cells to the fibronectin-positive area in every section (Fig. 6A). However, all pairs exhibited no significant differences ($P = 0.60$, $F_{(6,35)} = 1.56$, $n = 6$ mice; one-way ANOVA; Fig. 6B). Therefore, the ratios of fibronectin-positive cells in the fibronectin-positive area were nearly constant along the dorsoventral axis.

Furthermore, we sought to determine the functional relevance of fibronectin-positive cells in the subiculum. A previous study reported that vesicular glutamate transporter 2 (VGluT2) functions as a specific

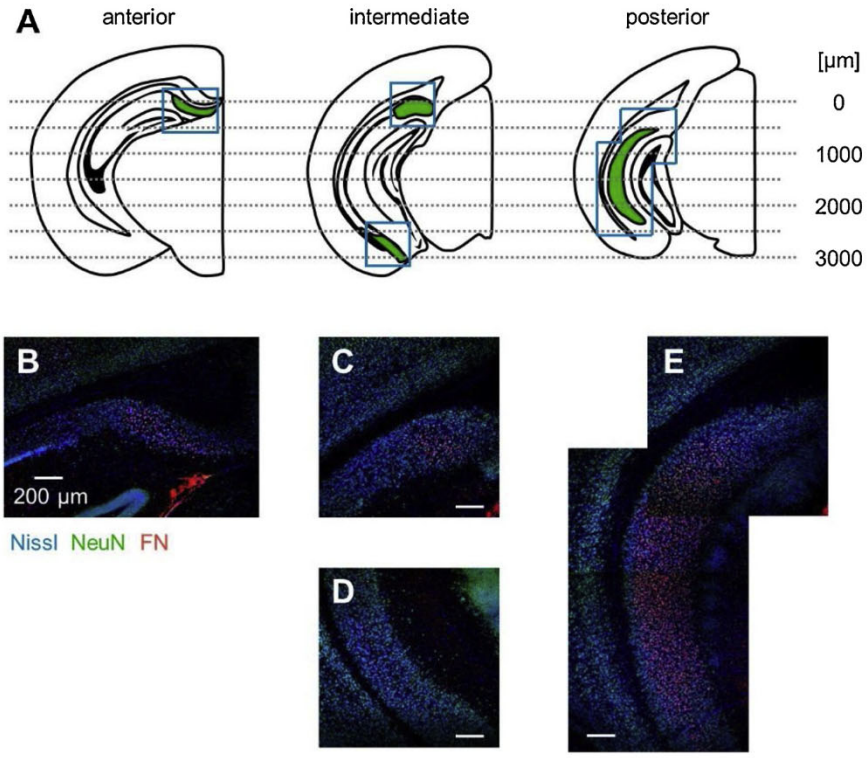

Fig. 5. Expression patterns of fibronectin in the coronal sections. *A*, Representative illustrations of anterior (*left*), intermediate (*middle*), and posterior (*right*) sections containing the subiculum (*green*). The numbers next to the *right* panel indicate distances (μm) from the most dorsal section. *B*, A representative immunohistochemical image of NeuN (*green*) and fibronectin (*red*) within the *blue*-boxed area in the anterior section shown as in *A*. *C*, The same as *B*, but for the dorsal subiculum in the intermediate section. *D*, The same as *B*, but for the ventral subiculum in the intermediate section. *E*, The same as *B*, but for the posterior section. *Abbreviation*: FN, fibronectin.

marker gene for bursting neurons in the subiculum (Wozny et al., 2018). Thus, we immunostained horizontal sections using antibodies against VGluT2 as well as fibronectin ($n = 3$ mice; Fig. 7). We found higher levels of VGluT2 expression in more ventral sections as opposed to the expression pattern of fibronectin (Fig. 7) and did not detect VGluT2 immunosignal in either the most dorsal or the most ventral sections (*data not shown*). This colocalization assay revealed that the expression of fibronectin and VGluT2 did not overlap (Fig. 7).

4. Discussion

Past studies have reported that FN1 mRNA, which encodes fibronectin, is expressed in the dorsal subiculum (Sheppard et al., 1995) and that the FN1 gene is expressed in the distal portion of the dorsal subiculum (Cembrowski et al., 2018a) but not in the ventral subiculum (Roy et al., 2017). Nevertheless, the expression of fibronectin, the protein encoded by the FN1 gene, has not been investigated in either the dorsal or the ventral subiculum. The current study provided a series of immunohistochemical images of fibronectin in the mouse subicular pyramidal cell layer along the dorsoventral axis. For horizontally sectioned slices, we propose several hypotheses: i) fibronectin is expressed not only in the dorsal but also in the ventral subiculum; ii) the dorsal subiculum expresses fibronectin more heavily than the ventral subiculum; iii) the distal portion of the subiculum expresses fibronectin more heavily than the proximal portion; iv) fibronectin is distributed homogeneously in the fibronectin-positive area along the dorsoventral axis.

We observed fibronectin in the dorsal and ventral subiculum, consistent with several previous mRNA studies (Cembrowski et al., 2018b; Roy et al., 2017; Sheppard et al., 1995). For instance, FN1 mRNA was expressed in pyramidal cells of the dorsal and ventral subiculum of mature mice (Cembrowski et al., 2018b). Moreover, Cre recombinase in

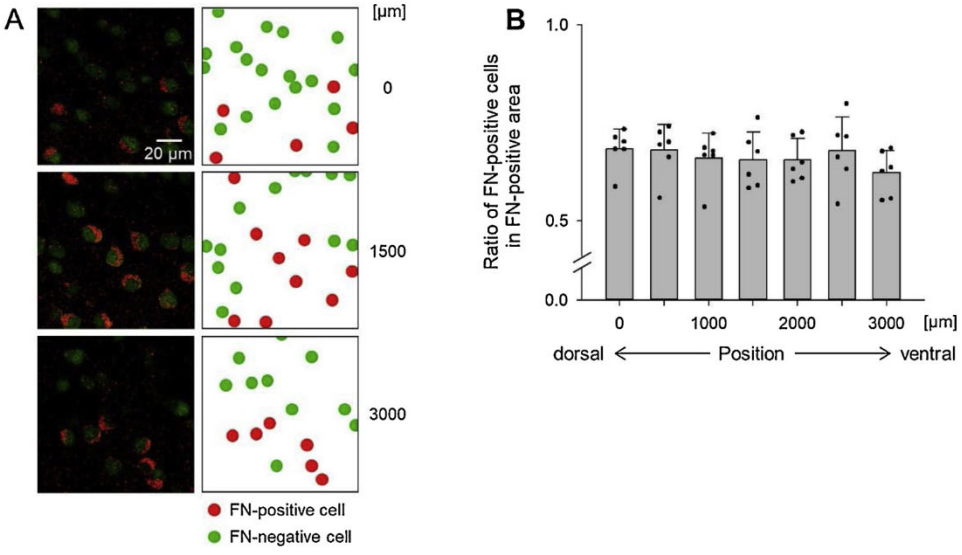

Fig. 6. Constant density of fibronectin-positive cells in the fibronectin-positive area along the dorsoventral axis. *A*, *Left*: representative high-magnification (40×) confocal images of the fibronectin-positive area in which anti-NeuN (*green*) and anti-fibronectin (*red*) images are superimposed. *Right*: scatter plots in which fibronectin-positive and fibronectin-negative cells are shown in *red* and *green*, respectively. The numbers indicate the distance from the most dorsal section (μm). *B*, The positions of the sections are indicated by the distance from the dorsal tip (0 μm). No significant differences were found between any pairs regarding the ratios of fibronectin-positive cells to the fibronectin-positive area ($P > 0.05$, one-way ANOVA, $n = 6$ mice each). The data are represented as the mean and SEM. *Abbreviation*: FN, fibronectin.

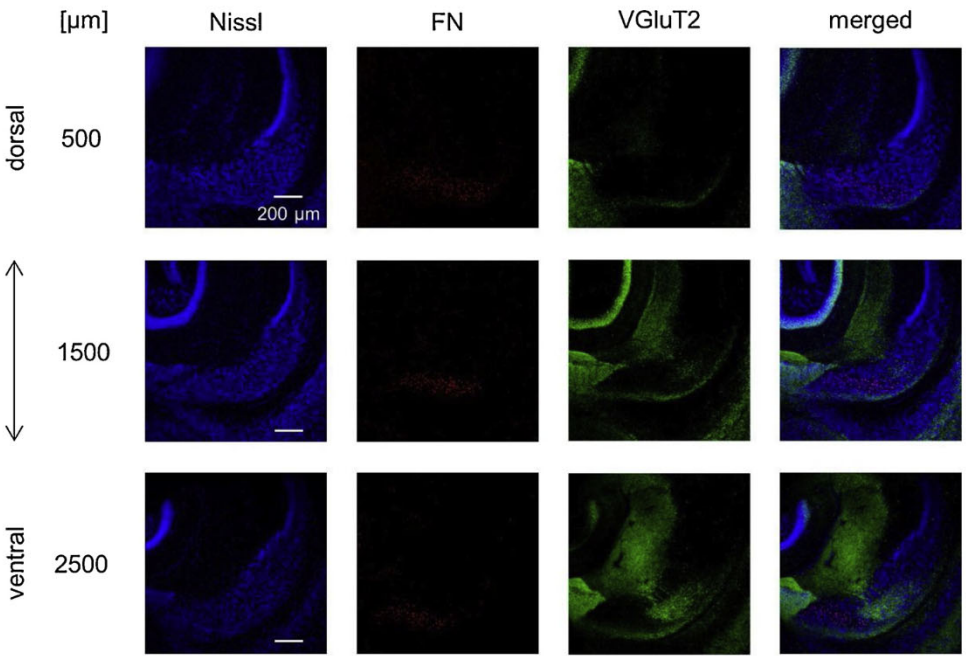

Fig. 7. Representative photographs of fibronectin and VGluT2 immunoreactivity in the subiculum of an adult mouse along the dorsoventral axis. In each row, confocal images of Nissl (*blue*, *left-most* column), anti-fibronectin (*red*, *second*), anti-VGluT2 (green, *third*) and merged (*fourth*) signal are shown. Different rows display photographs obtained from different dorsoventral levels, which are indicated as the distance (μm) from the most dorsal section. The experiments were repeated for all 3 animals of the same age, and the same results were obtained. *Abbreviation*: FN, fibronectin; VGluT2, vesicular glutamate transporter 2.

FN1-Cre mice was present in the dorsal subiculum (Roy et al., 2017). At the embryogenic level, FN1 mRNA in the dorsal subiculum was found from embryonic day 18 (Sheppard et al., 1995). In addition, a previous study reported that neuroepithelial expression of FN1 mRNA occurred throughout the telencephalon. Neuronal production of fibronectin was confined to cells migrating toward and into specific brain regions, including the subiculum. Fibronectin is completely confined to the subiculum once embryonic development is over (Sheppard et al., 1995).

We found that fibronectin was intracellularly expressed in the subiculum, whereas it was expressed outside the cell bodies in other regions. The expression patterns in brain regions other than the subiculum resemble those in peripheral organs. In peripheral organs, cellular fibronectin exists as a protein dimer. Cellular fibronectin is secreted as a soluble dimer and is then assembled into an insoluble extracellular matrix as a cell adhesion molecule (Dixon and Burns, 1982; Singh et al., 2010; Sottile and Hocking, 2002; Sottile and Wiley, 1994). One possible mechanism for fibronectin inside a cell might be a lack of transporters secreting fibronectin to the extracellular region.

As for the neurophysiological phenotype, subicular principal neurons are divided into regular-spiking and bursting neurons based on firing properties (Matsumoto et al., 2018). A recent study has shown that bursting neurons in the subiculum are immunolabeled by VGluT2 (Wozny et al., 2018). The colocalization assay for fibronectin and VGluT2 in the subiculum in our study revealed that fibronectin-positive and VGluT2-positive subareas were mutually exclusive (Fig. 7), suggesting that fibronectin-positive cells are regular-spiking neurons. Our experimental data bridge a gap between neuroanatomical and neurophysiological phenotypes; however, it is still unclear how intracellular fibronectin in the subiculum is related to cognitive functions, such as memory, learning, and spatial representation.

Previous studies have demonstrated that the firing rates of subicular regular-spiking neurons were reduced during CA1 ripples (Böhm et al., 2015) and that regular-spiking neurons exhibited experience-related plasticity in intrinsic excitability (Dunn et al., 2019). Further behavioral and electrophysiological assays combined with genetic manipulation will reveal the functional relevance of subicular fibronectin to spatial memory (Cembrowski et al., 2018a), nonspatial memory (Roy et al., 2017), and spatial representation (Lever et al., 2009; Olson et al., 2017).

Conflict of interest

The authors declare that they have no conflict of interest with respect to this research.

Ethical statement

Animal experiments were performed with the approval of the animal experiment ethics committee at the University of Tokyo (approval number: P24–10) and in accordance with the University of Tokyo guidelines for the care and use of laboratory animals. The experimental protocols were performed in accordance with the Fundamental Guidelines for the Proper Conduct of Animal Experiments and Related Activities in Academic Research Institutions (Ministry of Education, Culture, Sports, Science and Technology, Notice No. 71 of 2006), the Standards for Breeding and Housing of and Pain Alleviation for Experimental Animals (Ministry of the Environment, Notice No. 88 of 2006) and the Guidelines on the Method of Animal Disposal (Prime Minister's Office, Notice No. 40 of 1995).

Acknowledgments

This work was supported by JST ERATO (JPMJER1801), JSPS Grants-in-Aid for Scientific Research (18H05525), and the Human Frontier Science Program (RGP0019/2016). This work was conducted partly as a program at the International Research Center for Neurointelligence (WPI-IRCN) of The University of Tokyo Institutes for Advanced Study at The University of Tokyo.

References

Bienkowski, M.S., Bowman, I., Song, M.Y., Gou, L., Ard, T., Cotter, K., Zhu, M., Benavidez, N.L., Yamashita, S., Abu-Jaber, J., Azam, S., Lo, D., Foster, N.N., Hintiryan, H., Dong, H.W., 2018. Integration of gene expression and brain-wide connectivity reveals the multiscale organization of mouse hippocampal networks. Nat. Neurosci. 21, 1628–1643.

Böhm, C., Peng, Y., Maier, N., Winterer, J., Poulet, J.F., Geiger, J.R., Schmitz, D., 2015. Functional diversity of subicular principal cells during hippocampal ripples. J. Neurosci. 35, 13608–13618.

Cembrowski, M.S., Phillips, M.G., DiLisio, S.F., Shields, B.C., Winnubst, J., Chandrashekar, J., Bas, E., Spruston, N., 2018a. Dissociable structural and functional hippocampal outputs via distinct subiculum cell classes. Cell 173, 1280–1292.

Cembrowski, M.S., Wang, L., Lemire, A.L., Copeland, M., DiLisio, S.F., Clements, J.,

Spruston, N., 2018b. The subiculum is a patchwork of discrete subregions. eLife 7.
Chen, X., Shi, C., Wang, C., Liu, W., Chu, Y., Xiang, Z., Hu, K., Dong, P., Han, X., 2017. The role of miR-497-5p in myofibroblast differentiation of LR-MSCs and pulmonary fibrogenesis. Sci. Rep. 7, 40958.
Dixon, A.J., Burns, J., 1982. Ultrastructural localisation of fibronectin in mouse kidney. J. Pathol. 138, 25–31.
Dunn, A.R., Neuner, S.M., Ding, S., Hope, K.A., O'Connell, K.M., Kaczorowski, C.C., 2019. Cell-type-specific changes in intrinsic excitability in the subiculum following learning and exposure to novel environmental contexts. eNeuro 5 pii: ENEURO.0484-18.2018.
Fritschy, J.M., 2008. Is my antibody-staining specific? How to deal with pitfalls of immunohistochemistry. Eur. J. Neurosci. 28, 2365–2370.
Honda, Y., Ishizuka, N., 2015. Topographic distribution of cortical projection cells in the rat subiculum. Neurosci. Res. 92, 1–20.
Honda, Y., Shibata, H., 2017. Organizational connectivity among the CA1, subiculum, presubiculum, and entorhinal cortex in the rabbit. J. Comp. Neurol. 525, 3705–3741.
Ishihara, Y., Fukuda, T., 2016. Immunohistochemical investigation of the internal structure of the mouse subiculum. Neuroscience 337, 242–266.
Jarsky, T., Mady, R., Kennedy, B., Spruston, N., 2008. Distribution of bursting neurons in the CA1 region and the subiculum of the rat hippocampus. J. Comp. Neurol. 506, 535–547.
Lever, C., Burton, S., Jeewajee, A., O'Keefe, J., Burgess, N., 2009. Boundary vector cells in the subiculum of the hippocampal formation. J. Neurosci. 29, 9771–9777.
Matsumoto, N., Kitanishi, T., Mizuseki, K., 2018. The subiculum: unique hippocampal hub and more. Neurosci. Res.
Norimoto, H., Matsumoto, N., Miyawaki, T., Matsuki, N., Ikegaya, Y., 2013. Subicular activation preceding hippocampal ripples in vitro. Sci. Rep. 3, 2696.
Olson, J.M., Tongprasearth, K., Nitz, D.A., 2017. Subiculum neurons map the current axis of travel. Nat. Neurosci. 20, 170–172.
Reticker-Flynn, N.E., Malta, D.F., Winslow, M.M., Lamar, J.M., Xu, M.J., Underhill, G.H., Hynes, R.O., Jacks, T.E., Bhatia, S.N., 2012. A combinatorial extracellular matrix platform identifies cell-extracellular matrix interactions that correlate with metastasis. Nat. Commun. 3, 1122.
Rhodes, K.J., Trimmer, J.S., 2006. Antibodies as valuable neuroscience research tools versus reagents of mass distraction. J. Neurosci. 26, 8017–8020.
Roy, D.S., Kitamura, T., Okuyama, T., Ogawa, S.K., Sun, C., Obata, Y., Yoshiki, A., Tonegawa, S., 2017. Distinct neural circuits for the formation and retrieval of episodic memories. Cell 170, 1000–1012.
Sheppard, A.M., Brunstrom, J.E., Thornton, T.N., Gerfen, R.W., Broekelmann, T.J., McDonald, J.A., Pearlman, A.L., 1995. Neuronal production of fibronectin in the cerebral cortex during migration and layer formation is unique to specific cortical domains. Dev. Biol. 172, 504–518.
Singh, P., Carraher, C., Schwarzbauer, J.E., 2010. Assembly of fibronectin extracellular matrix. Annu. Rev. Cell Dev. Biol. 26, 397–419.
Sottile, J., Hocking, D.C., 2002. Fibronectin polymerization regulates the composition and stability of extracellular matrix fibrils and cell-matrix adhesions. Mol. Biol. Cell 13, 3546–3559.
Sottile, J., Wiley, S., 1994. Assembly of amino-terminal fibronectin dimers into the extracellular matrix. J. Biol. Chem. 269, 17192–17198.
van Strien, N.M., Cappaert, N.L., Witter, M.P., 2009. The anatomy of memory: an interactive overview of the parahippocampal-hippocampal network. Nat. Rev. Neurosci. 10, 272–282.
Worth, D.C., Hodivala-Dilke, K., Robinson, S.D., King, S.J., Morton, P.E., Gertler, F.B., Humphries, M.J., Parsons, M., 2010. αvβ3 integrin spatially regulates VASP and RIAM to control adhesion dynamics and migration. J. Cell Biol. 189, 369–383.
Wozny, C., Beed, P., Nitzan, N., Possnecker, Y., Rost, B.R., Schmitz, D., 2018. VGLUT2 functions as a differential marker for hippocampal output neurons. Front. Cell. Neurosci. 12, 337.
Yi, W., Xiao, E., Ding, R., Luo, P., Yang, Y., 2016. High expression of fibronectin is associated with poor prognosis, cell proliferation and malignancy via the NF-κB/p53-apoptosis signaling pathway in colorectal cancer. Oncol. Rep. 36, 3145–3153.